The role of *atoh1* genes in the development of the lower rhombic lip during zebrafish hindbrain morphogenesis

Ivan Belzunce and Cristina Pujades*

Department of Experimental and Health Sciences, Universitat Pompeu Fabra, 08003 Barcelona, Spain

*Correspondence to:
Cristina Pujades, PhD
Department of Experimental and Health Sciences
Universitat Pompeu Fabra
PRBB, Dr Aiguader 88, 08003 Barcelona, SPAIN
cristina.pujades@upf.edu
ORCID ID CP: 0000-0001-6423-7451

ABSTRACT

BACKGROUND: The Lower Rhombic Lip (LRL) is a transient neuroepithelial structure of the dorsal hindbrain, which expands from r2 to r7, and gives rise to deep nuclei of the brainstem, such as the vestibular and auditory nuclei and most posteriorly the precerebellar nuclei. Although there is information about the contribution of specific proneural-progenitor populations to specific deep nuclei, and the distinct rhombomeric contribution, little is known about how progenitor cells from the LRL behave during neurogenesis and how their transition into differentiation is regulated.

RESULTS: In this work, we investigated the *atoh1* gene regulatory network operating in the specification of LRL cells, and the kinetics of cell proliferation and behavior of *atoh1a*-derivatives by using complementary strategies in the zebrafish embryo. We unveiled that *atoh1a* is necessary and sufficient for specification of LRL cells by activating *atoh1b*, which worked as a differentiation gene to transition progenitor cells towards neuron differentiation in a Notch-dependent manner. This cell state transition involved the release of *atoh1a*-derivatives from the LRL: *atoh1a* progenitors contributed first to *atoh1b* cells, which are committed non-proliferative precursors, and to the *lhx2b*-neuronal lineage as demonstrated by cell fate studies and functional analyses. Using *in vivo* cell lineage approaches we showed that the proliferative cell capacity, as well as their mode of division, relied on the position of the *atoh1a* progenitors within the dorsoventral axis.

CONCLUSIONS: Our data demonstrates that the zebrafish provides an excellent model to study the *in vivo* behavior of distinct progenitor populations to the final neuronal differentiated pools, and to reveal the subfunctionalization of ortholog genes. Here, we unveil that *atoh1a* behaves as the cell fate selector gene, whereas *atoh1b* functions as a neuronal differentiation gene, contributing to the *lhx2b* neuronal population. *atoh1a*-progenitor cell dynamics (cell proliferation, cell differentiation, and neuronal migration) relies on their position, demonstrating the challenges that progenitor cells face in computing positional information from a dynamic two-dimensional grid in order to generate the stereotyped neuronal structures in the embryonic hindbrain.

KEYWORDS: neurogenesis, proneural genes, *atoh1*, hindbrain, rhombic lip, Notch

BACKGROUND

The assembly of functional neural circuits requires the specification of neuronal identities and the execution of developmental programs that establish precise neural network wiring. The generation of such cell diversity happens during embryogenesis, at the same time that the brain undergoes a dramatic transformation from a simple tubular structure, the neural tube, to a highly convoluted structure –the brain-, resulting in changes in the position of neuronal progenitors and their derivatives upon time. Thus, the coordination of progenitor proliferation and cell fate specification is central to tissue growth and maintenance.

The comprehension of how neuronal heterogeneity is achieved implies the understanding of how the neurogenic capacity is acquired, how the number of progenitors vs. differentiated neurons is balanced, and how their relative spatial distribution changes upon morphogenesis. Neurogenesis is initiated by proneural genes, which trigger the specification of neuronal lineages and commit progenitors to neuronal differentiation by promoting cell cycle exit and activating a downstream cascade of differentiation genes [1]. Once neuronal progenitors are committed, the first step towards achieving the diversity observed in adults occurs early in development with the division of neuronal progenitor cells into distinct domains along dorsoventral (DV) axis, which will give rise to different types of neurons in response to morphogen signals emanating from local organizing centers [2]. The next level of complexity arises within the interpretation of the two-dimensional grid, along the DV and anteroposterior (AP) axes, of molecularly distinct progenitor regions that will control the final neuronal fate.

The hindbrain undergoes a segmentation process along the AP axis leading to the formation of seven metameres named rhombomeres (r1-r7) that constitute developmental units of gene expression and cell lineage compartments [3-5]. This compartmentalization involves the formation of a cellular interface between segments called the hindbrain boundary [6], which exhibit distinct features such as specific gene expression [7] and biological functions [8-11]. The hindbrain is the most conserved brain vesicle along evolution [12,13], and in all vertebrates the dorsal part of the hindbrain gives rise to a transient neuroepithelial structure, the rhombic lip (RL). RL progenitors will generate different neuronal lineages according to their position along the AP axis.

The most anterior region of the RL, which coincides with the dorsal pole of r1, is known as Upper Rhombic Lip (UPL) and produces all granule cells of the external and internal granular layers of the cerebellum [14,15]. The rest of the RL, which expands from r2 to r7, is known as Lower Rhombic Lip (LRL) and gives rise to deep nuclei of the brainstem, such as the vestibular and auditory nuclei and most posteriorly the precerebellar nuclei [16,17]. The genetic program for cerebellum development is largely conserved among vertebrates [16]; as an example, zebrafish and mouse use similar mechanisms to control cerebellar neurogenesis with a crucial role of *atoh1* and *ptf1* genes [17,18]. For the LRL, we know both the contribution of *ptf1a/atoh1a* proneural progenitor populations to specific deep nuclei [19], and the distinct rhombomeric identity [20]. However, little is known about how progenitor cells from the LRL behave during neurogenesis and how their transition into differentiation is regulated, in order to balance the rate of differentiation and proliferation to produce the proper neuronal numbers.

In this work, we sought to understand the role of *atoh1* genes in the generation of the neuronal derivatives of LRL. We used complementary strategies in the zebrafish embryos to provide information about the gene regulatory network operating in the specification of LRL cells, and the kinetics of cell proliferation and behavior of *atoh1a*-derivatives. We unveiled that *atoh1a* is necessary and sufficient for specification of LRL cells by activating *atoh1b*, which worked as a differentiation gene to transition progenitor cells towards neuronal differentiation in a Notch-dependent manner. This cell state transition involved the release of *atoh1a*-derivatives from the LRL: *atoh1a* progenitors contributed first to *atoh1b* cells, which are committed non-proliferative precursors, and to the *lhx2b*-neuronal lineage as demonstrated by cell fate studies and functional analyses. Using *in vivo* cell lineage approaches we showed that the proliferative cell as well as their mode of division, relied on the position of the *atoh1a* progenitors within the dorsoventral axis.

RESULTS

Expression of proneural genes within the zebrafish hindbrain

We first analyzed the formation of molecularly distinct neural progenitor domains, each of them able to generate particular neuronal cell types, during hindbrain embryonic development. We performed a comprehensive spatiotemporal analysis of the expression of distinct proneural genes along the anteroposterior (AP) and dorsoventral (DV) axes within the hindbrain and defined the DV order of proneural gene expression. The expression profiles of *atoh1a*, *ptf1a*, *ascl1a*, *ascl1b*, and *neurog1* indicated that their onset of expression differed along the AP axis (Figure S1). The dorsal most progenitor cells express *atoh1a* all along the AP axis from 18hpf onwards, which remained expressed there until at least 48hpf (Figure S1A-C; Figure 1A-E). *ptf1a* expression started in rhombomere 3 (r3) at 18hpf and from 21hpf onwards it expanded anteriorly towards r1 and r2 (Figure S1D-E), ending up expressed all along the AP axis of the hindbrain with different intensities (Figure S1F; [17]). These two proneural genes were the most dorsally expressed as shown by transverse sections (Figure S1A'-C', D'-F'). *ascl1a* and *ascl1b* displayed overlapping expression profiles along the AP axis in a rhombomeric restricted manner with slightly different intensities (Figure S1G, J). Nevertheless, their DV expression differed: *ascl1a* expression was adjacently dorsal to *ascl1b* and constituted a smaller territory (Figure S1G'-I', J'-L', R). Indeed, *ascl1a* and *ptf1a* mainly overlapped along the DV axis occupying the region in between *atoh1a* and *ascl1b* (Figure S1P-R). Although by 24hpf *ascl1a*-cells seemed to be more laterally located than *ascl1b*-cells (compare Figure S1I with L), this just reflected the lateral displacement of dorsal part of the neural tube upon hindbrain ventricle opening: the hindbrain at early stages was a closed neural tube resembling the spinal cord (Figure S1, 18-21hpf stages), whereas al late stages all progenitor cells were in the ventricular zone faced the brain ventricle after lumen expansion (Figure S1C, 24hpf; compare Figure S2A'-B', E'-F' with C'-D', G'-H'). At 24hpf, *ascl1a/b* expression was restricted to rhombomeres, and by 42hpf their expression was clearly confined to the rhombomeric domains that flank the hindbrain boundaries (Figure S2A-D) as previously shown in [21,22]. Finally, *neurog1* was expressed in a more ventral position (Figure S1M-O, M'-O'), just below *ascl1a* (Figure S1S), and its expression restricted to the flanking boundary domains by 42hpf

(Figure S2E-H') [21]. Thus, by double *in situ* hybridization experiments we could assess the organization of the different proneural progenitor pools along the DV axis as following: *atoh1a*, *ptf1a/ascl1a*, *ascl1b*, *neurog1*, being *atoh1a*-cells the dorsal most progenitor cell population (Figure S1P-S). Interestingly, this was not the same order than proneural gene expression in the zebrafish spinal cord, where a second domain of *neurog1* progenitors positioned just underneath the *atoh1a* domain [23]. Proneural genes were expressed in non-differentiated progenitors, and accordingly, non-overlapping expression was observed with HuC-staining (Figure S2A'-H', Figure S3A', B-C). Interestingly, progenitors located in the dorsal most domain, became placed more lateral upon morphogenesis (see *atoh1a*-expressing cells in Figure 1E-E', Figure S3A'); and progenitors in the ventral region such as *neurog1*-cells, ended up in a more medial position (Figure S2E'-H'), showing the impact -and therefore the importance- of morphogenetic changes in the allocation of progenitor cells.

atoh1a and _atoh1b_ were sequentially expressed in partially overlapping domains

The three *atoh1* paralogs -*atoh1a, atoh1b* and *atoh1c*- were shown to be expressed within the hindbrain and to contribute to the development of the cerebellum, with the expression of *atoh1c* restricted to the upper rhombic lip [17,18]. Since our main interest was understanding the development of the lower rhombic lip (LRL), we focused on the study of *atoh1a* and *atoh1b* and compared their onset of expression. *atoh1a* preceded the expression of *atoh1b* in the most dorsal progenitor cells of the hindbrain at 14hpf (Figure 1A-A'). This was in contrast with the onset in the otic epithelium, where *atoh1b* was expressed earlier than *atoh1a* (see magenta in the otic placode in Figure 1A; [24]). At 18hpf, *atoh1a* expression remained in the dorsal most cells, whereas *atoh1b* expression domain was more lateral, overlapping with *atoh1a*-cells and mostly contained within this expression domain (Figure 1B-B', C-C'). Upon the opening of the neural tube, the *atoh1a/b* domains were laterally displaced and *atoh1a* remained medial whereas *atoh1b* positioned lateral (Figure 1D-D'), and by 42hpf -when the fourth ventricle was already formed- *atoh1b* expression was completely lateral, and *atoh1a* remained dorsal and medial (Figure 1E-E'). Thus, *atoh1a* and *atoh1b* were dorsally expressed but they differed in their mediolateral (apicobasal) position. To demonstrate that they were kept as progenitor cells, we stained Tg[HuC:GFP] embryos with *atoh1a/b*

and observed that neither *atoh1a* nor *atoh1b* were expressed in differentiated neurons (Figure 1F-H, F'-H'). Their differential apicobasal distribution and the fact that progenitor cell divisions always happened in the apical domains, suggested that *atoh1b*-progenitor cells might have experienced an apical displacement of their cell body before undergoing differentiation. To demonstrate this, we stained embryos with *atoh1a/b* and anti-pH3, a marker for mitotic figures, and observed that more *atoh1a* than *atoh1b* cells seemed to undergo mitosis (Figure 1I-I', J-J'). In this same line, the analyses of single mitotic cells in the transgenic Tg[atoh1a:GFP] fish line (Figure 1K-O) that labeled *atoh1a*-expressing cells and their derivatives [18], showed that mitotic atoh1a:GFP cells where always located in the ventricular domain (see white asterisks in Figure 1L-O, M'-O'), whereas the ones that did not divide were laterally displaced just above the neuronal differentiation domain (see black asterisks in Figure 1L-O, M'-O'). Thus, *atoh1b* cells may derive from *atoh1a* progenitors that diminished their proliferative capacity and behaved as committed progenitors transitioning towards differentiation.

atoh1a progenitors gave rise to _atoh1b_ cells and _lhx2b_ neurons

Next, we sought to unravel whether indeed *atoh1b* cells derived from *atoh1a* progenitors and which were the *atoh1a* neuronal derivatives. For this we used the same Tg[atoh1a:GFP] fish line than before [18], which allows to label the cell derivatives of *atoh1a* progenitors due the stability of GFP, and combined *in situ* hybridization experiments with immunostaining using *atoh1* probes, specific neuronal differentiation genes such as *lhx2b*, *lhx1a*, and pan-neuronal differentiation markers such as HuC (Figure 2, Figure S3). Although neuronal progenitors expressing *atoh1a* were restricted to the dorsal most region of the hindbrain, their derivatives were allocated in more ventral domains already at early stages of neuronal differentiation (Figure 2A-A', compare magenta and green domains). *atoh1b* cells, located more laterally than *atoh1a* cells, expressed GFP (Figure 2B-B', see white arrowhead in B' pointing to magenta/white cells in the green territory) indicating that indeed, they derived from *atoh1a* progenitors and according to their position they were transitioning towards differentiation. At this stage in which neuronal differentiation just started, ventral *atoh1a* derivatives constituted a lateral subgroup of differentiated neurons expressing the terminal factor *lhx2b* (see white asterisks indicating magenta/white cells in Figure 2C-C'). Note that the

more medial *lhx2b* neurons in r4 did not arise from *atoh1a* cells (Figure 2C, see white arrowhead, and compare it with D). This was expected because the lateral domain of *lhx2b* cells always fell below the *atoh1a* progenitors (Figure S3A'), when compared to the more medial domain falling underneath *ascl1b* cells (Figure S3A', B). When the pan-neuronal differentiation marker HuC was analyzed (Figure 2E-F), we could clearly observe that at these early stages *atoh1a* derivatives contributed to a portion of differentiated cells (compare Figure 2E-E', with F-F'). Thus, the Tg[atoh1a:GFP] line labeled several cell populations: i) two progenitor cell pools -the one expressing *atoh1a*, and another expressing *atoh1b*-, and ii) the lateral domain of differentiated *lhx2b* neurons. By 48hpf, most of the *atoh1a* progenitors have differentiated, and the remaining *atoh1a/b* progenitor pools were very small (Figure 2G-H, G'-H'). Although *lhx2b* neurons occupied two territories, one lateral and one medial (see white asterisk and arrowhead in Figure S3A-A', respectively), the *atoh1a* derivatives specifically contributed to the most laterally located *lhx2b* neurons (see white asterisk pointing to magenta/white cells in Figure 2I-I'; see white asterisks in Figure S3A-A') and did not give rise to the medial *lhx2b* neurons (see white arrowhead in Figure 2I-I') or *lhx1a* neurons (Figure S3B). Concomitantly to the growth of the HuC-positive mantle zone, the neuronal differentiation domains dramatically increased (see white and magenta domains in Figure 2K-K', L-L', respectively; see green domains in Figure S2C'-D', G'-H'). As expected, cells organized properly along the DV axis according to their differentiation state: progenitor cells in the ventricular domain and cells transitioning towards differentiation more ventrally located (Figure S3C-C''). To better understand the dynamics of atoh1a-derived neurons, we *in vivo* monitored how the atoh1a:GFP cells populated the ventral domain of the hindbrain. We observed that the first-born *atoh1a* neurons occupied the rhombomeric edges or boundary regions (see white arrowhead in Figure S4A-C; Figure 2D). By 48hpf, *atoh1a*-derivatives already populated the basal domain of the hindbrain (at this morphogenetic stage ventrally located), generating arched-like structures that coincided with rhombomeric boundaries (see yellow arrowhead in Figure 2G-L, see white arrowheads in Figure S4), implying that once the dorsal progenitors commit, they undergo cellular migration during differentiation.

In summary, *atoh1a* progenitors gave rise to *atoh1b* cells and to the lateral domain of *lhx2b* neurons. First differentiated *atoh1a* cells placed between rhombomeres to finally populate the basal hindbrain and generate arched-liked structures.

Reconstruction of the *atoh1a* lineage

Next question was to address how the rate of differentiation and proliferation of *atoh1a* cells was balanced to achieve the needed cell diversity. For this, we used genetic lineages that allowed to delineate cell types arising from *atoh1a* subsets. To trace the *atoh1a* neuronal lineages we used a transgenic line that expressed the H2A-mCherry fluorescent reporter protein under the control of enhancer elements of the *atoh1a.* Tg[atoh1a:H2A-mCherry] fish were crossed with Tg[CAAX:GFP] -to have the contour of the cells- and embryos at 24hpf were imaged over 14h. Information about plasma membrane, cell fate and position was simultaneously recorded every 7min (Figure 3A as an example). We monitored the *atoh1a* progenies and studied their behavior according to their position along the DV axis to (Figure 3B-E). We tracked 40 *atoh1a*-cells, 22 dorsal most (see cells encircled in orange in Figure 3B) and 20 adjacently ventral (see cells encircled in white in Figure 3C), and analyzed their trajectories, when and how many times they divided during the 14h that they were imaged (Figure 3D), and by which mode of division they did so (Figure 3E) attending to their morphology and location: symmetrically giving rise to two progenitor cells (PP) or two neurons (NN), or asymmetrically generating one progenitor cell and one neuron (NP). Of the 22 tracked dorsal most cells (Figure 3B, D), only 59% of them divided, and they did so only once (Figure 3D, orange bars; n = 13/22). On the other hand, 82% of cells located just in the underneath domain underwent cell division either once or twice (Figure 3C-D, white bars; n = 14/17). Dorsal most *atoh1a* cells undergoing division gave rise always to two cells ending up as differentiated neurons (Figure 3E, dorsal cells NN n=13/13), whereas the *atoh1a* cells located just below divided according to the three modes of division: 35% gave to two progenitor cells (Figure 3E, ventral cells PP n = 7/20) or two differentiated neurons (Figure 3E, ventral cells NN n = 7/20), and 30% displayed an asymmetric division (Figure 3E, ventral cells NP n=6/20). These results demonstrated that the dorsal most domain allocated *atoh1a* cells already transitioning towards

differentiation, whereas the proliferating *atoh1a*-progenitor pool occupied the region just underneath, generating a dorsoventral gradient of neuronal differentiation.

atoh1a **is necessary and sufficient for neuronal specification**

Our observations suggested that proliferating *atoh1a* progenitors gave rise to post-mitotic *atoh1b* precursors and *lhx2b* neurons in a sequential manner. However, in order to elucidate the hierarchy between these factors and cellular types, we analyzed the effect of *atoh1a* mutation on the neuronal differentiation domain (Figure 4). We made use of the available *atoh1a*^{fh282} mutant fish in the Tg[atoh1a:GFP] background, which carried a missense mutation within the DNA-binding domain [18]. First, we observed that mutation of *atoh1a* resulted in a complete loss of *atoh1b* expression within the hindbrain (Figure 4A-A', D-D', G-G', J-J'), suggesting that *atoh1a* was necessary for *atoh1b* expression and supporting the previous result that *atoh1b* cells derived from *atoh1a* progenitors. This phenotype was accompanied with the loss of the most lateral *lhx2b*-neuronal population (see white asterisk in Figure 4B-B', E-E', H-H', K-K'), but not of the *lhx2b*-medial column in r4 that remained unaffected (see white arrowhead in Figure 4B-B', E-E', H-H', K-K'), as it was anticipated since this specific population of *lhx2b* neurons did not derive from the *atoh1a* cells (Figure 2D). Although the overall pattern of neuronal atoh1a:GFP cells was not dramatically changed (Figure 4C-C', F-F', I-I', L-L'), when the number of neurons at different AP positions was assessed we could observe a clear decrease in the number of differentiated *atoh1a* neurons in the *atoh1a*^{fh282} mutant embryos at both the onset and progression of neuronal differentiation (Figure 4M-N, quantification of green dashed inserts in Figure 4C, F, I, L; Table 1).

To address the possibility that the decrease in the number of neurons in *atoh1a*^{fh282} mutants was the result of a smaller number of *atoh1a* progenitor cells, we quantified the number of LRL atoh1a:GFP cells undergoing mitosis (Figure 5A), and the overall number of atoh1a:GFP cells (Figure 5B), both in *atoh1a*^{WT} and *atoh1a*^{fh282} embryos. No significative differences were observed, suggesting that loss of atoh1a function did not affect the original number of LRL progenitors (Figure 5A; LRL atoh1a:GFP cells displaying PH3-staining: *atoh1a*^{WT} 17.9 ± 3.6 cells n = 15 vs. *atoh1a*^{fh282} 15.9 ± 3.1 cells, n = 8; Figure 5B; total atoh1a:GFP cells: *atoh1a*^{WT} 69.5 ± 6.4 cells n = 15 vs. *atoh1a*^{fh282} 68.4 ± 7.5 cells, n = 8; see Table 2). Since the domains of neural bHLH gene expression are established

and/or maintained by cross-repression resulting in the control of specific neuronal populations [1], we sought whether this neuronal loss was due to a change in cell fate rather than to a reduction of the number of progenitor cells. Thus, we analyzed proneural gene expression changes both in wild type and mutant context (Figure 5C-F; *atoh1a*^{WT} n = 8, *atoh1a*^{fh282} n = 10). We observed that upon *atoh1a* mutation, *atoh1a* expression dramatically increased as previously reported [18] (compare Figure 5C and F) and the GFP-expressing progenitor cells did not die (Figure 5D-D', G-G'). In addition, these cells remained in an intermediate domain since they did not completely migrate towards their final ventral destination as they did in *atoh1a*^{WT} embryos (compare Figure 5D' and G'; see white arrow in Figure 5F'-H'). When we analyzed their possible cell fate switch, by assessing whether the GFP-expressing progenitor cells in the mutant context acquired the expression of the adjacent proneural gene *ptf1a*, atoh1a:GFP progenitors in the *atoh1a*^{fh282} embryos did not display *ptf1a* expression (compare Figure 5E-E' and H-H', see white arrow in H'). These observations indicated that in the absence of atoh1a function cells remained as post-mitotic but undifferentiated progenitors, and the LRL domain was properly specified since no changes in the number of cells was observed.

Loss of atoh1a function resulted in accumulation of atoh1a:GFP progenitors unable to migrate and finally differentiate. In order to demonstrate that these committed precursors arrested, we performed high-resolution time-lapse imaging of both *atoh1a*^{WT} and *atoh1a*^{fh282} embryos from 24hpf onwards and followed the birth and migration of these atoh1a:GFP progenitors (Figure 5I-J). Before migrating, *atoh1a* progenitors in the wild type context, extended their apical and basal feet along the mediolateral axis of the neuroepithelium (dorsal stacks in Figure 5I; white asterisk indicating the tracked cell), and then moved away from the dorsal epithelium towards the mantle zone where they resided as differentiated neurons (see ventral stacks in Figure 5I; white asterisk indicating the tracked cell). This transition was accomplished in an average period of 4.5h (Figure 5I, K; t = 275min ± 102; n = 28 tracked cells). In contrast, *atoh1a*^{fh282} progenitors failed to transition and detach (see dorsal stacks in Figure 5J; white asterisk indicating the tracked cell) to barely migrate basally (see medial stacks in Figure 5J; white asterisk indicating the tracked cell). Indeed, after 9.5h of imaging most of *atoh1a*^{fh282} cells still remained in the dorsomedial epithelial region (Figure 5J-K; t = 569min ± 180; n

= 9/12 tracked cells). Thus, our observations revealed that *atoh1a* was necessary for initial steps of neuronal differentiation (apical abscission and migration).

To further demonstrate the requirement of *atoh1a* in *atoh1b* expression and *lhx2b* neuronal differentiation, and better dissect the proneural gene hierarchy, we performed conditional gain of function experiments. We injected Mu4127 embryos expressing Gal4 in r3 and r5 with H2B-citrine:UAS vectors carrying either *atoh1a* or *atoh1b* genes, and analyzed the effects in *atoh1* genes and *lhx2b* neurons (Figure 6, Table 3). The *atoh1a* transgene proved successful, as *atoh1a* expression was spread along the DV axis, where it induced the expression of *atoh1b* (compare Figure 6 A'-B' and D'-E') as well as ectopic *lhx2b* neurons in r5 (compare Figure 6C' and F'), a rhombomere usually devoid of these neurons at this stage. This was a cell autonomous effect, since all cells expressing *atoh1b* or *lhx2b* ectopically expressed Citrine, and therefore *atoh1a* (compare green cells in Figure 6E-H with magenta cells in E'-H'). On the other hand, although *atoh1b* expression resulted in ectopic *lhx2b* induction (Figure 6H'-I') it did not activate *atoh1a* expression (Figure 5G'), demonstrating that *atoh1b* and *atoh1a* were not interchangeable, and *atoh1a* was upstream *atoh1b*. Overall, our results proved that *atoh1a* progenitors activated *atoh1b,* which allowed them to transition towards differentiation and contribute to the *lhx2b* neuronal population. Moreover, these experiments demonstrated the neurogenic potential of *atoh1b*, and importantly, its role in assigning a neuronal identity subtype.

Notch-signaling regulates the transition of *atoh1a* cycling progenitors towards *atoh1b* committed cells

We showed that *atoh1a* cycling cells gave rise to *atoh1b* post-mitotic committed precursors. Since this commitment is suspected to be irreversible and leading towards neuronal differentiation, we thought the Notch signaling pathway as a reasonable candidate to be regulating this transition. Thus, we explored the Notch activity within the LRL to understand how *atoh1b* expression was restricted to a given *atoh1a*-domain in the neural tube. First, we assessed Notch activity by the use of the Tg[tp1:d2GFP] transgenic line, which is a readout of Notch-active cells [25]. Indeed, Notch-activity was restricted to the most dorsomedial *atoh1a* cell population (Figure 7A-A'), whereas the more laterally located *atoh1b* cells were devoid of it (Figure 7B-B'). This suggested that

Notch activity was responsible of preventing *atoh1a* progenitor cells to transition to *atoh1b* and therefore modulating neuronal differentiation. To demonstrate this, we conditionally inhibited Notch activity by incubating Tg[atoh1a:GFP] embryos with the gamma-secretase inhibitor LY411575, and asked whether *atoh1a/b* expression domains were altered. Upon inhibition of Notch activity, there was an increase of *atoh1b*-expression at expense of *atoh1a* (Figure 7C-D, F-G): *atoh1b* expression was expanded more medially, and *atoh1a* expression dramatically decreased (compare the border of the *atoh1b* expression in Figure 7D' with G'). As expected, the *atoh1b* cells did not arise *de novo* but derived from atoh1a:GFP progenitors (Figure 7E-E', H-H'), supporting the idea that Notch-pathway regulated the transition of *atoh1a* progenitors towards differentiation.

DISCUSSION

Progenitor cell populations undergo important changes in their relative spatial distribution upon morphogenesis, which need to be precisely coordinated with the balance between progenitor cells vs. differentiated neurons. Here, we have defined the role of *atoh1* genes along the development of the LRL population, and how this progenitor cell population behaves during the early neurogenic phase.

The spatiotemporal activation of proneural genes in the hindbrain shows that the neurogenic capacity is regionalized along the AP axis, such as that hindbrain boundaries and rhombomere centers remain devoid of neurogenesis [22]. This is valid for most of proneural genes except for *atoh1* genes, because these are expressed all along the AP axis in the dorsal most hindbrain; however, RL derivatives delaminate from the dorsal epithelium, migrate and transitorily locate in the boundary regions. Interestingly, our results demonstrate that the function of different *atoh1* genes depends on the context. In the inner ear, *atoh1a* and *atoh1b* cross-regulate each other but are differentially required during distinct developmental periods: *atoh1b* activates *atoh1a* early, whereas in a late phase *atoh1a* maintains *atoh1b* [24]. In the URL, *atoh1a* and *atoh1c* have equivalent function in the generation of granular cells progenitors [18], whereas we argue that in the LRL *atoh1a* and *atoh1b* are not interchangeable, since they work directionally and have distinct functions. Although in the URL *atoh1a* activates the expression of *neurod1* in intermediate, non-proliferative precursors [26], *neurod1* expression is not detected in the zebrafish LRL before the 48hpf, implying that *atoh1b* is the one defining LRL intermediate precursors rather than *neurod1* during early LRL-derived neurogenesis.

Zebrafish has three *atoh1* genes, *atoh1a, atoh1b* and *atoh1c*, which are expressed in overlapping but distinct progenitor domains within the rhombic lip [17,18]. Although *atoh1a* and *atoh1c* specify different, non-overlapping pools of progenitors within the UPL, in the LRL while *atoh1b* largely overlaps with *atoh1a* it defines a cellular state rather than a progenitor lineage. *atoh1b* is expressed in a cell population that derives from *atoh1a* progenitors, and it has diminished its proliferative capacity; thus, *atoh1b* cells experienced an apical displacement of their cell body behaving as committed progenitors transitioning towards differentiation. This observation implies that *atoh1*

gene duplication in teleosts resulted in a gene sub-functionalization: *atoh1a* behaves as the cell fate selector gene, whereas *atoh1b* functions as a neuronal differentiation gene maintaining the transcriptional program initiated by *atoh1a*. In our conditional functional experiments, *atoh1a* ectopic expression was rapidly downregulated, whereas ectopic *atoh1b* remained active at later stages, highlighting the different roles of *atoh1a* and *atoh1b* in initiating vs. maintaining the differentiation program.

Recently, it has been shown that nuclei in the hindbrain start migrating from variable apicobasal positions and move toward the apical surface in a directed and smooth manner, and this movement is controlled by Rho-ROCK–dependent myosin contractility [27]. However, the mechanisms by which actin generates the forces required for apical nuclear movement and the link between forces and *atoh1b* are not understood.

Interestingly, first-born neurons from the LRL delaminate and migrate towards medio-ventral positions to allocate in rhombomeric boundaries. Later-born LRL neurons follow the same trajectory, pile up with them and settle more laterally generating what we call neuronal arch-like structures. We think that this pattern of neuronal organization responds to some kind of chemo-attractant signal derived from boundary cells, as first *atoh1a* derivatives have a tendency to allocate within rhombomeric boundaries independently from their AP position upon differentiation. Many of such signalling pathways have been described for LRL migrating cells in the mouse embryo [28]; however, signals participating in this particular context are unknown. Nonetheless, boundary cells are signalling centres instructing the neuronal allocation in the neighbouring tissue [9]; thus, one plausible hypothesis is that boundary cells might dictate the allocation of newly-differentiated neurons.

Balancing the rate of differentiation and proliferation in developing neural tube is essential for the production of appropriate numbers and achieving the needed cell diversity to form a functional central nervous system (CNS). This requires a finely tuned balance between the different modes of division that neural progenitor cells undergo [29]. Three distinct modes of divisions occur during vertebrate CNS development: self-expanding (symmetric proliferative, PP) divisions ensure the expansion of the progenitor pool by generating two daughter cells with identical progenitor potential, self-renewing (asymmetric, PN) divisions generate one daughter cell with the same developmental potential than the parental cell and another with a more restricted potential, and self-

consuming (symmetric terminal neurogenic, NN) divisions generate two cells committed to differentiation, thereby depleting the progenitor pool [29,30]. Our *in vivo* cell lineage studies shed light into this specific question in respect to the *atoh1a* cell population. We reveal the importance of the initial allocation of *atoh1a* progenitors: dorsal most *atoh1a* progenitors display more neurogenic capacity than ventral ones, since they give rise only to NN divisions upon the early neurogenic phase, whereas *atoh1a* progenitors located just underneath undergo the three distinct modes of division ensuring the expansion of the *atoh1a*-pool and providing committed progenitors. Most probably, the originally located dorsal progenitors will quickly become *atoh1b* and transition towards differentiation allocating more laterally. Interestingly, in the amniote spinal cord the modes of progenitor division are coordinated over time [31], instead of space. Why such a difference? One explanation is that in the LRL, where the position of progenitor cells changes dramatically over time, the most efficient way to provide fast neuronal production without exhausting the pool of progenitors could be regionalising the proliferative capacity. On the other hand, *in vivo* experiments in the chick spinal cord showed that an endogenous gradient of SMAD1/5 activity dictated the mode of division of spinal interneuron progenitors, in such a way that high levels of SMAD1/5 signalling promoted PP divisions, whereas a reduction in SMAD1/5 activity forced spinal progenitors to reduce self-expanding divisions in favour of self-consuming divisions [32]. This would suggest that dorsal most *atoh1a* cells would respond less to BMP signalling than ventral *atoh1a* cells. However, during hindbrain morphogenesis there is an important change in the position of *atoh1a* progenitors, and therefore their relative position in respect to the gradient sources. Since morphogen gradients quickly decrease with distance [33,34], it is difficult to apply the same rationale here than in the spinal cord. Still very little is known about how these gradients are established within the hindbrain [35], and how hindbrain progenitors interpret the quantitative information encoded by the concentration and duration of exposure to gradients. An alternative explanation is that different E proteins may control the ability of *atoh1a* to instruct dorsal or ventral neural progenitor cells to produce specific, specialized neurons, and thus ensure that the distinct types of neurons are produced in appropriate amounts as it happens in the chick spinal cord [36].

The loss of *atoh1a* function clearly affects the formation of the lateral column of *lhx2b* differentiated neurons and decreases the number of overall differentiated neurons. But what are the derivatives of these *atoh1a*-derived *lhx2b* cells? It has been described that the hindbrain displays a striking organization into transmitter stripes reflecting a broad patterning of neurons by cell type, morphology, age, projections, cellular properties, and activity patterns [37]. According to this pattern, the lateral *lhx2b* column would correspond to glutamatergic neurons expressing the *barhl2* transcription factor [37], which in turn is an *atoh1a* target [38,39].

Notch has been extensively studied as a regulator of proneural gene expression by a process called lateral inhibition, in which cells expressing higher levels of proneural genes are selected as “neuroblasts” for further commitment and differentiation, while concomitantly maintaining their neighbors as proliferating neural precursors available for a later round of neuroblast selection [40]. Indeed, in the LRL the transition *atoh1a* to *atoh1b* seems to be regulated by Notch-activity, since upon Notch-inhibition most of the *atoh1a* cells disappear and they become *atoh1b*, and therefore are ready to undergo differentiation. Thus, although *atoh1a* is the upstream factor in LRL cell specification, several mechanisms seem to be in place to precisely coordinate acquisition of the neurogenic capacity and progenitor vs. differentiation transitions.

CONCLUSIONS

Our data demonstrates that the zebrafish provides an excellent model to study the contribution of distinct progenitor populations to the final neuronal differentiated pools, and to reveal the subfunctionalization of ortholog genes. We unveil that *atoh1a* behaves as the cell fate selector gene, whereas *atoh1b* functions as a neuronal differentiation gene, contributing to the *lhx2b* neuronal population. *atoh1a*-progenitor cell dynamics (cell proliferation, cell differentiation, and neuronal migration) relies on their position, demonstrating the challenges that progenitor cells face in computing positional information from a dynamic two-dimensional grid in order to generate the stereotyped neuronal structures in the embryonic hindbrain.

METHODS

Zebrafish lines and genotyping

Zebrafish (*Dario rerio*) were treated according to the Spanish/European regulations for the handling of animals in research. All protocols were approved by the Institutional Animal Care and Use Ethic Committees and implemented according to European regulations. Experiments were carried out in accordance with the principles of the 3Rs. Embryos were obtained by mating of adult fish using standard methods. All zebrafish strains were maintained individually as inbred lines. The transgenic line Mu4127 carries the KalTA4-UAS-mCherry cassette into the 1.5Kb region downstream of *egr2a/krx20* gene, and was used for targeting UAS-constructs to rhombomeres 3 and 5, or as landmark of these regions [41]. Tg[βactin:HRAS-EGFP] line, called Tg[CAAX:GFP] in the manuscript, displays GFP in the plasma membrane and was used to label the cell contours [42]. Tg[tp1:d2GFP] line is a readout of cells displaying Notch-activity [25] in which cells with active Notch express GFP. The Tg[HuC:GFP] line labels differentiated neurons [43]. Tg[atoh1a:Kalta4;UAS:H2A-mCherry] and Tg[atoh1a:Kalta4;UAS:GFP] fish lines label *atoh1a*-positive cells and their derivatives due to the stability of the fluorescent proteins. They were generated by crossing Tg[atoh1a:Gal4] [44] with Tg[UAS:H2A-mCherry] or Tg[UAS:GFP] lines, respectively, and accordingly were called Tg[atoh1a:H2A-mCherry] and Tg[atoh1a:GFP] all along the manuscript for simplification. *atoh1a*^{fh282} mutant line in the Tg[atoh1a:GFP] background, which carried a missense mutation within the DNA-binding domain, was previously described in [18]. Embryos were phenotyped blind and later genotyped by PCR using the following primers: Fw primer 5'-ATGGATGGAATGAGCACGGA-3' and Rv primer 5'-GTCGTTGTCAAAGGCTGGGA-3'. Amplified PCR products underwent digestion with AvaI (New England Biolabs), which generated two bands: 195 bp + 180 bp for the WT allele and 195 bp + 258 bp for the mutant allele. Since the *atoh1a*^{fh282} mutant allele only caused a deleterious phenotype in homozygosity, wild type and heterozygous conditions showed identical phenotypes and they were displayed in all our experiments as a single wild type condition.

Whole mount *in situ* hybridization and immunostainings

Zebrafish whole-mount *in situ* hybridization was adapted from [45]. The following riboprobes were generated by *in vitro* transcription from cloned cDNAs: *atoh1a* and *atoh1b* [24], *ptf1a, ascl1a, ascl1b* [46], *neurog1* [47], and *neurod4* [48]. *lhx1a* and *lhx2b* probes were generated by PCR amplification adding the T7 promoter sequence in the Rv primers (*lhx2b* Fw primer, 5'-CAG AGA CGA ACA TGC CTT CA-3'; *lhx2b* Rv primer, 5'-ATA TTA ATA CGA CTC ACT ATA CGT CAG GAT TGT GGT TAG ATG -3'; *lhx1a* Fw primer, 5'-CCA GCT ACA GGA CGA TGT CA-3'; *lhx1a* Rv primer, 5'-ATA TTA ATA CGA CTC ACT ATA GAG GGA CGT AAA AGG ACG GAC T-3'). The chromogenic *in situ* hybridizations were developed with NBT/BCIP (blue) substrate. For fluorescent *in situ* hybridization, FLUO- and DIG-labeled probes were detected with TSA Fluorescein and Cy3, respectively.

For immunostaining, embryos were blocked in 5% goat serum in PBS-Tween20 (PBST) during 1h at room temperature and then incubated O/N at 4°C with the primary antibody. The primary antibodies were the following: anti-GFP (1:200; Torrey Pines), anti-pH3 (1:200; Upstate), anti-HuC (1:100, Abcam). After extensive washings with PBST, embryos were incubated with secondary antibodies conjugated with Alexa Fluor®594 or Alexa Fluor®633 (1:500, Invitrogen). Either Draq5™ (1:2000; Biostatus, DR50200) or DAPI were used to label nuclei. After staining, embryos were either flat-mounted and imaged under a Leica DM6000B fluorescence microscope, or whole-mounted in agarose and imaged under a SP8 Leica confocal microscope.

Quantification of the phenotypes

For quantifying the number of differentiated neurons in *atoh1a*^{WT}Tg[atoh1a:GFP] and *atoh1a*^{fh282}Tg[atoh1a:GFP] embryos, confocal MIP of ventral stacks were used and all cells present in the r4/r5 and r5/r6 domain were counted (Figure 4M-N; see Table 1 for numbers and statistics).

In order to quantify the number of proliferating LRL-cells in *atoh1a*^{WT} and *atoh1a*^{fh282} embryos in the Tg[atoh1a:GFP] background, the number of mitotic figures within the atoh1a:GFP progenitor domain was assessed (Figure 5A; see Table 2 for numbers and statistics).

For the quantification of the total number of LRL atoh1a:cells in *atoh1a*^{WT} and *atoh1a*^{fh282} embryos in the Tg[atoh1a:GFP] background, embryos were stained with

Draq5 and the total number of nuclei of atoh1a:GFP cells was assessed in r5 (Figure 5B; see Table 2 for numbers and statistics).

For the quantification of the delamination time of atoh1a:cells in *atoh1a*^{WT} and *atoh1a*^{fh282} embryos in the Tg[atoh1a:GFP] background, we kept track of the time of division of a given cell (t0) and the time of delamination of the resulting cells (tf) and calculated the difference between tf and t0 (Figure 5K).

3D+time imaging

Double transgenic Tg[atoh1a:H2A-mCherry]TgCAAX:GFP] embryos (Figure 3), or *atoh1a*^{WT}Tg[atoh1a:GFP] and *atoh1a*^{fh282}Tg[atoh1a:GFP] embryos (Figure 5I-K) were anesthetized and mounted dorsally in 1%LMP-agarose. Time-lapse imaging was performed from 24hpf to 34hpf in a Leica SP8 system using PMT detectors and a 20x objective. Experimental parameters for the videos were: voxel dimension (nm), x416.6 y416.6 z1200; time frame 8 min; total time 14 h; pinhole 1 Airy; zoom 1.3; objective 20x immersion; NA 0.70. The videos were processed and analyzed using Fiji software (NIH). Cell tracking was performed using the MaMuT software (Fiji plug-in) [49].

Conditional overexpression

The full-length coding sequences of zebrafish *atoh1a*- and *atoh1b* [24] were cloned into the MCS of a custom dual vector that expressed Citrine from one side of 5xUAS sequence and the cDNA of interest from the opposite side [21]. Mu4127 embryos (expressing KalT4 in r3 and r5) were injected either with H2B-citrine:UAS, H2B-citrine:UAS:atoh1a or H2B-citrine:UAS:atoh1b constructs at the one-cell stage, grown at 28.5°C and analyzed at 24hpf for *atoh1a/b* and *lhxb2 in situ* hybridization and Citrine expression.

Pharmacological treatments

Tg[atoh1a:GFP] embryos were treated either with 10μM of the gamma-secretase inhibitor LY411575 (Stemgent) or DMSO for control. The treatment was applied into the swimming water at 28.5°C from 24hpf to 30hpf. After treatment, embryos were fixed in 4%PFA for further analysis.

DECLARATIONS

Ethics approval and consent to participate

Zebrafish (*Dario rerio*) were treated according to the Spanish/European regulations for the handling of animals in research. All protocols were approved by the Institutional Animal Care and Use Ethic Committees and implemented according to European regulations. Experiments were carried out in accordance with the principles of the 3Rs. Embryos were obtained by mating of adult fish using standard methods.

Consent for publication

Not applicable.

Availability of data and materials

Most of the data generated or analyzed during this study are included in this published article [and its supplementary information files]. However, the imaging datasets used and/or analyzed in Figure 3-5 are available from the corresponding author on reasonable request.

Competing interests

The authors IB and CP declare no competing financial interests.

Funding

This work was supported by Spanish Ministry of Economy and Competitiveness BFU2015-67400-P to CP, and BFU2016-81887-REDT/AEI (MINECO-FEDER), and Unidad de Excelencia María de Maetzu MDM-2014-0370 to DCEXS-UPF. IB was a recipient of a predoctoral FI fellowship (AGAUR, Generalitat de Catalunya). CP is recipient of an ICREA Academia award (Institució Catalana per la Recerca i Estudis Avançats, Generalitat de Catalunya).

Authors' contributions

IB and CP contributed to the concept and design of experiments, and analysis of the results. IB performed all the experiments. CP wrote the manuscript.

Acknowledgements

We thank R Köster, B Link, and C Moens who kindly provided us with transgenic lines. We would like to thank L Subirana and M Linares for technical assistance, and the members of Pujades lab for critical insights, in special C Engel-Pizcueta and C Belmonte who generated the UAS:H2A-mCherry transgenic line.

REFERENCES

1. Bertrand N, Castro DS, Guillemot F. Proneural genes and the specification of neural cell types. Nature Reviews Neuroscience. 2002;3:517–30.

2. Ribes V, Briscoe J. Establishing and Interpreting Graded Sonic Hedgehog Signaling during Vertebrate Neural Tube Patterning: The Role of Negative Feedback. Cold Spring Harbor Perspectives in Biology. 2009;1:a002014–4.

3. Kiecker C, Lumsden A. Compartments and their boundaries in vertebrate brain development. Nature Reviews Neuroscience. 2005;6:553–64.

4. Fraser S, Keynes R, Lumsden A. Segmentation in the chick embryo hindbrain is defined by cell lineage restrictions. Nature. 1990;344:431–5.

5. Jimenez-Guri E, Udina F, Colas J-F, Sharpe J, Padrón-Barthe L, Torres M, et al. Clonal analysis in mice underlines the importance of rhombomeric boundaries in cell movement restriction during hindbrain segmentation. Winkler C, editor. PLoS ONE. Public Library of Science; 2010;5:e10112.

6. Guthrie S, Lumsden A. Formation and regeneration of rhombomere boundaries in the developing chick hindbrain. Development. 1991;112:221–9.

7. Letelier J, Terriente J, Belzunce I, Voltes A, Undurraga CA, Polvillo R, et al. Evolutionary emergence of therac3b/rfng/sgcaregulatory cluster refined mechanisms for hindbrain boundaries formation. Proc. Natl. Acad. Sci. U.S.A. 2018.

8. Calzolari S, Terriente J, Pujades C. Cell segregation in the vertebrate hindbrain relies on actomyosin cables located at the interhombomeric boundaries. EMBO J. EMBO Press; 2014;33:686–701.

9. Terriente J, Gerety SS, Watanabe-Asaka T, Gonzalez-Quevedo R, Wilkinson DG. Signalling from hindbrain boundaries regulates neuronal clustering that patterns neurogenesis. Development. 2012;139:2978–87.

10. Peretz Y, Eren N, Kohl A, Hen G, Yaniv K, Weisinger K, et al. A new role of hindbrain boundaries as pools of neural stem/progenitor cells regulated by Sox2. BMC Biol. BioMed Central; 2016;14:57.

11. Voltes A, Hevia CF, Engel-Pizcueta C, Dingare C, Calzolari S, Terriente J, et al. Yap/Taz-TEAD activity links mechanical cues to progenitor cell behavior during zebrafish hindbrain segmentation. Development. 2019;146.

12. Murakami Y, Uchida K, Rijli FM, Kuratani S. Evolution of the brain developmental plan: Insights from agnathans. Developmental Biology. 2005;280:249–59.

13. Jimenez-Guri E, Pujades C. An ancient mechanism of hindbrain patterning has been conserved in vertebrate evolution. Evolution & Development. Blackwell Publishing Inc; 2011;13:38–46.

14. Volkmann K, Rieger S, Babaryka A, Köster RW. The zebrafish cerebellar rhombic lip is spatially patterned in producing granule cell populations of different functional compartments. Developmental Biology. 2008;313:167–80.

15. Volkmann K, Chen Y-Y, Harris MP, Wullimann MF, Köster RW. The zebrafish cerebellar upper rhombic lip generates tegmental hindbrain nuclei by long-distance migration in an evolutionary conserved manner. J. Comp. Neurol. John Wiley & Sons, Ltd; 2010;518:2794–817.

16. Hibi M, Matsuda K, Takeuchi M, Shimizu T, Murakami Y. Evolutionary mechanisms that generate morphology and neural-circuit diversity of the cerebellum. Develop. Growth Differ. 2017.

17. Kani S, Bae Y-K, Shimizu T, Tanabe K, Satou C, Parsons MJ, et al. Proneural gene-linked neurogenesis in zebrafish cerebellum. Developmental Biology. 2010;343:1–17.

18. Kidwell CU, Su C-Y, Hibi M, Moens CB. Multiple zebrafish atoh1 genes specify a diversity of neuronal types in the zebrafish cerebellum. Developmental Biology. 2018;438:44–56.

19. Fujiyama T, Yamada M, Terao M, Terashima T, Hioki H, Inoue YU, et al. Inhibitory and excitatory subtypes of cochlear nucleus neurons are defined by distinct bHLH transcription factors, Ptf1a and Atoh1. Development. 2009;136:2049–58.

20. Farago AF, Awatramani RB, Dymecki SM. Assembly of the Brainstem Cochlear Nuclear Complex Is Revealed by Intersectional and Subtractive Genetic Fate Maps. Neuron. 2006;50:205–18.

21. Nikolaou N, Watanabe-Asaka T, Gerety S, Distel M, Köster RW, Wilkinson DG. Lunatic fringe promotes the lateral inhibition of neurogenesis. Development. 2009;136:2523–33.

22. Gonzalez-Quevedo R, Lee Y, Poss KD, Wilkinson DG. Neuronal regulation of the spatial patterning of neurogenesis. Developmental Cell. 2010;18:136–47.

23. Satou C, Kimura Y, Hirata H, Suster ML, Kawakami K, Higashijima S-I. Transgenic tools to characterize neuronal properties of discrete populations of zebrafish neurons. Development. 2013;140:3927–31.

24. Millimaki BB, Sweet EM, Dhason MS, Riley BB. Zebrafish atoh1 genes: classic proneural activity in the inner ear and regulation by Fgf and Notch. Development. 2007;134:295–305.

25. Clark BS, Cui S, Miesfeld JB, Klezovitch O, Vasioukhin V, Link BA. Loss of Llgl1 in retinal neuroepithelia reveals links between apical domain size, Notch activity and neurogenesis. Development. 2012;139:1599–610.

26. Iulianella A, Wingate RJ, Moens CB, Capaldo E. The generation of granule cells during the development and evolution of the cerebellum. Dev. Dyn. John Wiley & Sons, Ltd; 2019;248:506–13.

27. Yanakieva I, Erzberger A, Matejčić M, Modes CD, Norden C. Cell and tissue morphology determine actin-dependent nuclear migration mechanisms in neuroepithelia. J Cell Biol. 2019.

28. Kratochwil CF, Maheshwari U, Rijli FM. The Long Journey of Pontine Nuclei Neurons: From Rhombic Lip to Cortico-Ponto-Cerebellar Circuitry. Front Neural Circuits. 2017;11:33.

29. Franco SJ, Müller U. Shaping our minds: stem and progenitor cell diversity in the mammalian neocortex. Neuron. 2013;77:19–34.

30. Lui JH, Hansen DV, Kriegstein AR. Development and evolution of the human neocortex. Cell. 2011;146:18–36.

31. Saade M, Gutiérrez-Vallejo I, Le Dréau G, Rabadán MA, Miguez DG, Buceta J, et al. Sonic hedgehog signaling switches the mode of division in the developing nervous system. Cell Reports. 2013;4:492–503.

32. Le Dréau G, Saade M, Gutiérrez-Vallejo I, Martí E. The strength of SMAD1/5 activity determines the mode of stem cell division in the developing spinal cord. J Cell Biol. Rockefeller University Press; 2014;204:591–605.

33. Kicheva A, Cohen M, Briscoe J. Developmental Pattern Formation: Insights from Physics and Biology. Science. 2012;338:210–2.

34. Kicheva A, Bollenbach T, Ribeiro A, Valle HP, Lovell-Badge R, Episkopou V, et al. Coordination of progenitor specification and growth in mouse and chick spinal cord. Science. 2014;345:1254927–7.

35. Hernandez-Miranda LR, Müller T, Birchmeier C. The dorsal spinal cord and hindbrain: From developmental mechanisms to functional circuits. Developmental Biology. 2017;432:34–42.

36. Le Dréau G, Escalona R, Fueyo R, Herrera A, Martínez JD, Usieto S, et al. E proteins sharpen neurogenesis by modulating proneural bHLH transcription factors' activity in an E-box-dependent manner. Elife. 2018;7:8730.

37. Kinkhabwala A, Riley M, Koyama M, Monen J, Satou C, Kimura Y, et al. A structural and functional ground plan for neurons in the hindbrain of zebrafish. Proc. Natl. Acad. Sci. U.S.A. National Acad Sciences; 2011;108:1164–9.

38. Kawauchi D, Saito T. Transcriptional cascade from Math1 to Mbh1 and Mbh2 is required for cerebellar granule cell differentiation. Developmental Biology. Elsevier Inc; 2008;322:345–54.

39. Klisch TJ, Xi Y, Flora A, Wang L, Li W, Zoghbi HY. In vivo Atoh1 targetome reveals how a proneural transcription factor regulates cerebellar development. Proc. Natl. Acad. Sci. U.S.A. 2011;108:3288–93.

40. Chitnis AB. Control of neurogenesis--lessons from frogs, fish and flies. Current Opinion in Neurobiology. 1999;9:18–25.

41. Distel M, Wullimann MF, Köster RW. Optimized Gal4 genetics for permanent gene expression mapping in zebrafish. Proc. Natl. Acad. Sci. U.S.A. National Acad Sciences; 2009;106:13365–70.

42. Dale RM, Topczewski J. Identification of an evolutionarily conserved regulatory element of the zebrafish col2a1a gene. Developmental Biology. 2011;357:518–31.

43. Park HC, Kim CH, Bae YK, Yeo SY, Kim SH, Hong SK, et al. Analysis of upstream elements in the HuC promoter leads to the establishment of transgenic zebrafish with fluorescent neurons. Developmental Biology. 2000;227:279–93.

44. Distel M, Hocking JC, Volkmann K, Köster RW. The centrosome neither persistently leads migration nor determines the site of axonogenesis in migrating neurons in vivo. J Cell Biol. Rockefeller University Press; 2010;191:875–90.

45. Thisse C, Thisse B, Schilling TF, Postlethwait JH. Structure of the zebrafish snail1 gene and its expression in wild-type, spadetail and no tail mutant embryos. Development. 1993;119:1203–15.

46. Allende ML, Weinberg ES. The expression pattern of two zebrafish achaete-scute homolog (ash) genes is altered in the embryonic brain of the cyclops mutant. Developmental Biology. 1994;166:509–30.

47. Itoh M, Chitnis AB. Expression of proneural and neurogenic genes in the zebrafish lateral line primordium correlates with selection of hair cell fate in neuromasts. MECHANISMS OF DEVELOPMENT. 2001;102:263–6.

48. Park S-H, Yeo S-Y, Yoo K-W, Hong S-K, Lee S, Rhee M, et al. Zath3, a neural basic helix-loop-helix gene, regulates early neurogenesis in the zebrafish. BIOCHEMICAL AND BIOPHYSICAL RESEARCH COMMUNICATIONS. 2003;308:184–90.

49. Wolff C, Tinevez J-Y, Pietzsch T, Stamataki E, Harich B, Guignard L, et al. Multi-view light-sheet imaging and tracking with the MaMuT software reveals the cell lineage of a direct developing arthropod limb. Elife. 2018;7.

TABLE 1

Quantification of the number of differentiated cells in *atoh1a*^{WT} and *atoh1a*^{fh282} embryos at 24hpf and 36hpf with the t-test values (see Figure 4M-N).

	atoh1a^{WT}	n	*atoh1a*^{fh282}	n	p
r4/r5-24hpf	20.5 ± 4	14	1.4 ± 1.9	11	< 0.001
r5/r6-24hpf	11.9 ± 3.3	14	0.25 ± 0.7	11	< 0.001
r4/r5-36hpf	85.8 ±18.2	18	26.7 ± 9.5	7	< 0.001
r5/r6-36hpf	75.6 ± 21.1	18	25.1 ± 11.9	7	< 0.001

TABLE 2

Quantification of LRL cells in *atoh1a*^{WT} and *atoh1a*^{fh282} embryos at 24hpf with the t-test values (see Figure 5A-B).

	atoh1a^{WT}	n	*atoh1a*^{fh282}	n	p
mitotic atoh1a:GFP LRL cells	17.9 ± 3.6	15	15.9 ± 3.1	8	ns
total LRL atoh1a:GFP cells	69.5 ± 6.4	15	68.4 ± 7.5	8	ns

TABLE 3

Analysis of the phenotypes in gain-of-function experiments (Figure 6).

Numbers indicate the of embryos displaying a phenotype as the one shown in Figure 6, over the total number of analyzed embryos (X/Y).

	atoh1a	*atoh1b*	*lhx2b*
H2B-citrine:UAS	16/16	13/13	18/18
H2B-citrine:UAS:atoh1a	35/35	18/25	12/13
H2B-citrine:UAS:atoh1b	16/16	28/28	10/14

FIGURE LEGENDS

Figure 1: Spatiotemporal analysis of *atoh1a* and *atoh1b* within the hindbrain.

A-E) Whole mount double *in situ* hybridization with *atoh1a* (green) and *atoh1b* (magenta) in wild type embryos from 14hpf to 42hpf. Dorsal views with anterior to the left. A'-E') Reconstructed transverse views of dorsal views in (A-E) at the level indicated by the white arrow depicted in (A-E). Note that the expression of *atoh1b* is more lateral than *atoh1a*-cells. Dotted line corresponded to the neural tube contour. F-H) Whole mount double *in situ* hybridization with *atoh1a* (green) and *atoh1b* (magenta) on Tg[HuC:GFP] embryos from 24hpf to 42hpf, where HuC expression was displayed in white. Dotted line corresponded to the neural tube and the HuC-expression contours (only half of it). I-J) Embryos at 30hpf were double *in situ* hybridized with *atoh1a* (green) and *atoh1b* (magenta) and cell proliferation was assessed by anti-PH3 staining (white). Dorsal views with anterior to the left. I'-J') Reconstructed transverse views of (I-J) at the level pointed by the white arrow in (I-J). Note *atoh1a*-cells underwent mitosis, whereas fewer *atoh1b*-cells did. Dotted line corresponded to the neural tube contour. K) Tg[atoh1a:GFP] embryo (green) after anti-PH3 (magenta) and DAPI (blue) staining in dorsal view with anterior to the left. L, N) Magnification of the R1 and R2 regions framed in (K), displaying an example of apical atoh1a:GFP cells undergoing division (white asterisk) and lateral atoh1a:GFP cells that did not (black asterisk). M-M', O-O') Reconstructed transverse views of (L) and (N), respectively, with (M,O) or without (M', O') the red-PH3 staining, in order to show the position of the given atoh1a:GFP cells within the DV axis. Note that atoh1a:GFP cell nuclei expressing PH3 are located in the apical region, whereas atoh1a:GFP cell nuclei negative for PH3 (most probably *atoh1b*-positive) are in the most lateral domain. op, otic placode; ov, otic vesicle; r, rhombomere. Scale bars correspond to 50μm.

Figure 2: Analysis of the *atoh1a* neuronal derivatives in Tg[atoh1a:GFP] embryos.

Tg[atoh1a:GFP] embryos at 24hpf and at 48hpf were assayed for *atoh1a* (A, G), *atoh1b* (B, H), *lhx2b* (C-D, I-J) *in situ* hybridization, and anti-HuC (E-F, K-L) staining. Dorsal views of confocal MIP from dorsal stacks (A-B) or ventral stacks (C-L) with anterior to the left. A'-L') Reconstructed transverse sections of the dorsal views in (A-L) at the level indicated

with the white arrow depicted in (A-L) corresponding to r4/r5. All embryos displayed the *atoh1a*-progenitors and derivatives in green. Note that *atoh1b* cells derive from atoh1a:GFP progenitors (B', H'), as well as the lateral *lhx2b* neuronal domain (see white asterisks in C', I-I'), whereas the medial *lhx2b* neuronal column in r4 is devoid of green staining (see white arrowhead in C, I-I'). See that differentiated neurons organize in arch-like structures (yellow arrowhead in G-L). ov, otic vesicle; SAG, statoacoustic ganglion; r, rhombomere. Scale bars correspond to 50μm.

Figure 3: Cell lineages and behavior of *atoh1a*-derivatives.

Tg[atoh1a:H2A-mCherry] Tg[CAAX:GFP] embryos were imaged from 24hpf during 14h, and information about cell position was acquired every 7min. A) Dorsal view of an embryonic hindbrain displaying *atoh1a* cells in magenta with anterior to the left. The inserts display magnified stills from the framed area in (A) at different times (see white arrow as example of a cell that was tracked from t0 to t100). Note the cell nucleus displacement towards the apical side before division (t8). B-C) Cell lineages from r4 and r5 *atoh1a*-progenitors located at different dorsoventral levels within the *atoh1a* domain; n = 22 in (B) and n = 17 in (C). Each line corresponds to a single cell that branches upon division. Lines are colored according to cell differentiation status: progenitors in grey and differentiated cells in green. The X-axis corresponds to developmental time. The right-hand images display examples of the trajectories of the *atoh1a* tracked cells (white arrow) on the top of the transverse views at t0 (24hpf). Cell trajectories are color-coded according to cell differentiation status: progenitors are in white and differentiated neurons in green. Dorsal most *atoh1a* cells are encircled in orange and ventral *atoh1a* cells are encircled in white. D) Histogram displaying the number of most dorsal (orange) or ventral (white) atoh1a:GFP cells that undergo different number of divisions over time. Note that *atoh1a*-cells that are more dorsally located undergo less division rounds (orange bars) than the ones in a more ventral position (white bars). E) Mode of cell division according to the DV position of the *atoh1a*-progenitor cells. NN, progenitors giving rise to two neurons; NP, progenitors generating one neuron and one progenitor; PP, progenitor cells that give rise to two progenitors. Note that most dorsal *atoh1a* cells give rise to differentiated cells in all analyzed cases (n = 22 *atoh1a* progenitors), whereas *atoh1a* cells more ventrally located employ the three modes of

division (n = 17 *atoh1a* progenitors). nt, lumen of the neural tube; ov, otic vesicle; r, rhombomere.

Figure 4: *atoh1a* is required for the specification of the *lhx2b* neuronal population.
A-L) *atoh1a*^{WT} and *atoh1a*^{fh282} embryos in the Tg[atoh1a:GFP] background were analyzed at 24hpf (*atoh1a*^{WT} n = 14; *atoh1a*^{fh282} n = 18) and 36hpf (*atoh1a*^{WT} n = 11; *atoh1a*^{fh282} n = 7) with *atoh1b* (A, D, G, J), *lhx2b* (B, E, H, K), and anti-GFP in order to follow the *atoh1a*-derivatives (C, F, I, L). A'-L') Reconstructed transverse views of dorsal views displayed in (A-L) at the level of the anterior side of the otic vesicle. Note that *atoh1b* expression (compare A-A' and G-G' with D-D' and J-J'), and the lateral domains of *lhx2b* diminished (compare white asterisks in B-B' with E-E', and H-H' with K-K'), whereas the more medial domain does not decrease so dramatically (compare white arrowheads in B-B' with E-E', and H-H' with K-K'). Note that atoh1a:GFP cells remained, suggesting that there is no massive cell death. M-N) Quantification of differentiated neurons in the r4/r5 and r5/r6 domains of *atoh1a*^{WT} and *atoh1a*^{fh282} embryos as depicted in the small inserts showing dorsal views of halves hindbrains that correspond to the framed regions in (F-L), *** $p<0.001$ (Table 1 for values and statistical analysis). Note the reduction in the number of atoh1a:GFP differentiated neurons in *atoh1a*^{fh282} embryos. ov, otic vesicle; r, rhombomere. Scale bars correspond to 50μm.

Figure 5: *atoh1a*^{fh282} mutation does not result in changing the cell fate or cell loss.
A-B) Box-plots with the quantification of mitotic figures within the LRL atoh1a:GFP cells (A), and the total number of LRL atoh1a:GFP cells (B), in *atoh1a*^{WT} and *atoh1a*^{fh282} embryos. Note that no differences between wild type and mutant embryos was observed (Table 2 for values and statistical analysis). D-E) *atoh1a*^{WT} (n = 8) and (F-H) *atoh1a*^{fh282} (n = 10) embryos in the Tg[atoh1a:GFP] background were concomitantly analyzed for *atoh1a* (C, F), *atoh1a*-derivatives visualized with anti-GFP staining (D, G) and *ptf1a* (E, H) expression. C'-H') Reconstructed transverse views of dorsal views displayed in (C-H) at the level of the otic vesicle. Note that the atoh1a:GFP cells in the *atoh1a*^{fh282} mutant did not migrate towards the differentiation domain and did not display *ptf1a* (see white arrow in F'-H'), indicating that progenitor cells did not switch fate. I-J) Time-lapse stills showing delamination from the LRL of tracked atoh1a:GFP

cells (indicated with white asterisk) in *atoh1a*^{WT} (n = 28) and *atoh1a*^{fh282} (n = 12) embryos in the Tg[atoh1a:GFP] background. Dorsal views of hemi-neural tubes (dashed white line indicates the apical region of the hindbrain), with anterior to the left and lateral at the top. Numbers at the top-right indicate the minutes after the beginning of the movie. Note that in wild type embryos, the cell delaminates and migrates towards ventral allocating in the corresponding neuronal differentiation zone (see the first three dorsal frames and then the following ventral ones), whereas in *atoh1a*^{fh282} embryos the indicated cell remains within the dorsal epithelium (see that there are four dorsal frames and two medial because the cell never reaches ventral). K) Box-plot indicating the time of delamination from the LRL of atoh1a:GFP cells in *atoh1a*^{WT} and *atoh1a*^{fh282} embryos. Note that cells from in wild types exit the LRL much earlier than in mutants. Since the *atoh1a*^{fh282} mutant allele only caused a deleterious phenotype in homozygosity, wild type and heterozygous conditions showed identical phenotypes and they were displayed as single wild type condition. nt; neural tube lumen; ov, otic vesicle. Scale bars correspond to 50μm. ns, non-statistically significant; *** p<0.001.

Figure 6: *atoh1a* is upstream of *atoh1b* and is necessary for *lhxb2* neurons.

Mu4127 embryos expressing Gal4 in rhombomeres 3 and 5 were injected with H2B-citrine:UAS (A-C), H2B-citrine:UAS:atoh1a (D-F) or H2B-citrine:UAS:atoh1b (G-I) constructs in order to ectopically express the gene of interest in r3 and r5. Injected embryos were assayed for Citrine expression (green) and *atoh1a* (A-A', D-D', G-G'), *atoh1b* (B-B', E-E', H-H') or *lhx2b* (C-C', F-F', I-I') expression (magenta). Reconstructed transverse views displaying the merge of the red and green channels (A-I), or only the red channel (A'-I'). Note that ectopic expression of *atoh1a* in more ventral domains induces *atoh1b* and *lhxb2* expression (see white arrowheads in D-F, D'-F'), whereas ectopic *atoh1b* expression induces *lhx2b* but not *atoh1a* (see white arrowheads in H-I, H'-I'). See Table 3 for numbers of analyzed embryos. r, rhombomere. Scale bars correspond to 50μm.

Figure 7: Notch-signaling regulates the transition of *atoh1a* cycling progenitors towards *atoh1b* committed cells.

A-B) Whole mount double *in situ* hybridization with *atoh1a* (green) and *atoh1b* (magenta) in Tg[tp1:GFP] embryos (readout of Notch-activity in white). A'-B') Reconstructed transverse views of embryos displayed as dorsal views in (A-B) through the point indicated by the white arrow in (A-B). Note that Notch-activity is restricted to the most dorsomedial tip of the hindbrain, corresponding with *atoh1a* cells. C-H) Tg[atoh1a:GFP] embryos were double *in situ* hybridized with *atoh1a* (green) and *atoh1b* (magenta) after treatment with DMSO (C-E, n = 10) or the gamma-secretase inhibitor LY411575 (F-H, n = 15). The *atoh1a* derivatives were followed by anti-GFP staining in white. C'-H') Reconstructed transverse views of embryos displayed as dorsal views in (C-H) at the level indicated by the white arrow in (C-H). Note how the *atoh1b*-domain expands at expense of *atoh1a* progenitors after blocking Notch-activity. A-D, F-G) Dorsal views of confocal MIP from dorsal stacks with anterior to the left. E, H) Dorsal views of confocal MIP from ventral hindbrain with anterior to the left. ov, otic vesicle. Scale bars correspond to 50μm.

SUPPLEMENTARY FIGURES

Suppl Figure 1: Proneural gene expression within the zebrafish embryonic hindbrain.
Whole mount *in situ* hybridization at 18hpf, 21hpf and 24hpf using *atoh1a* (A-C, Q), *ptf1a* (D-F, P), *ascl1a* (G-I, P-S), *ascl1b* (J-L, R) and *neurog1* (M-O, S) probes. Dorsal views with anterior to the left. A'-O') Transverse views at the level pointed by the black arrowhead of embryos displayed in (A-O). P-S) Transverse views of double *in situ* hybridized embryos with the indicated probes. ov, otic vesicle; r, rhombomere.

Suppl Figure 2: Expression of *ascl1b* and *neurog1* proneural genes along the dorsoventral axis in the context of the neuronal differentiation domain.
Tg[HuC:GFP] embryos were *in situ* hybridized with *ascl1b* (A-D) or *neurog1* (E-H) from 24hpf until 48hpf. A-H) Dorsal views with anterior to the left; A'-H') Reconstructed transverse views at the level pointed by the white arrow in (A-H). Note that progenitor domain in magenta diminishes in size and constitutes the ventricular zone as neuronal differentiation increases over time. ov, otic vesicle. Scale bars correspond to 50μm.

Suppl Figure 3: Comparison of the progenitor and differentiated domains upon morphogenesis.
Tg[HuC:GFP] embryos were *in situ* hybridized either with *atoh1a* and *lhx2b* (A-A'), *ascl1b* and *lhx1a* (B), or *ascl1b* and *neuroD4* (C-C''). Reconstructed transverse views except for (A), which is a dorsal view, showing the distinct position of progenitors (*atoh1a* or *ascl1b* in magenta) and differentiated neurons (*lhx2b* and *lhx1a* in green), and cells transitioning towards differentiation (*neuroD4* in green) along the DV axis. ov, otic vesicle; r, rhombomere. Scale bars correspond to 50μm.

Suppl Figure 4: First born *atoh1a* cells allocate within the rhombomeric boundaries.
A-E) Double transgenic Tg[atoh1a:GFP]Mu4127 embryos were *in vivo* imaged at different developmental stages. Dorsal views of confocal MIP from ventral hindbrain with anterior to the left. Note that most of the first born atoh1a:GFP cells (green) at 21hpf position at the rhombomeric boundaries as indicated by the magenta staining in r3 and r5 (see white arrowheads indicating the most ventral atoh1a:GFP derivatives).

Later, more atoh1a:GFP cells are generated and populate the whole AP axis (see white asterisks in (B-E)) piling up with the first-born atoh1a:GFP cells (see white asterisks). A'-E', A''-E'') Reconstructed transverse views of (A-E) at the level of r4/r5 displaying either the two channels (A'-E') or only the green one (A''-E''). See how the atoh1a:GFP cells corresponding to *atoh1a*-derivatives end up generating a neuronal arch-like structure (see white arrowheads) as development proceeds. ov, otic vesicle; r, rhombomere. Scale bars correspond to 50μm.

FIGURE 1

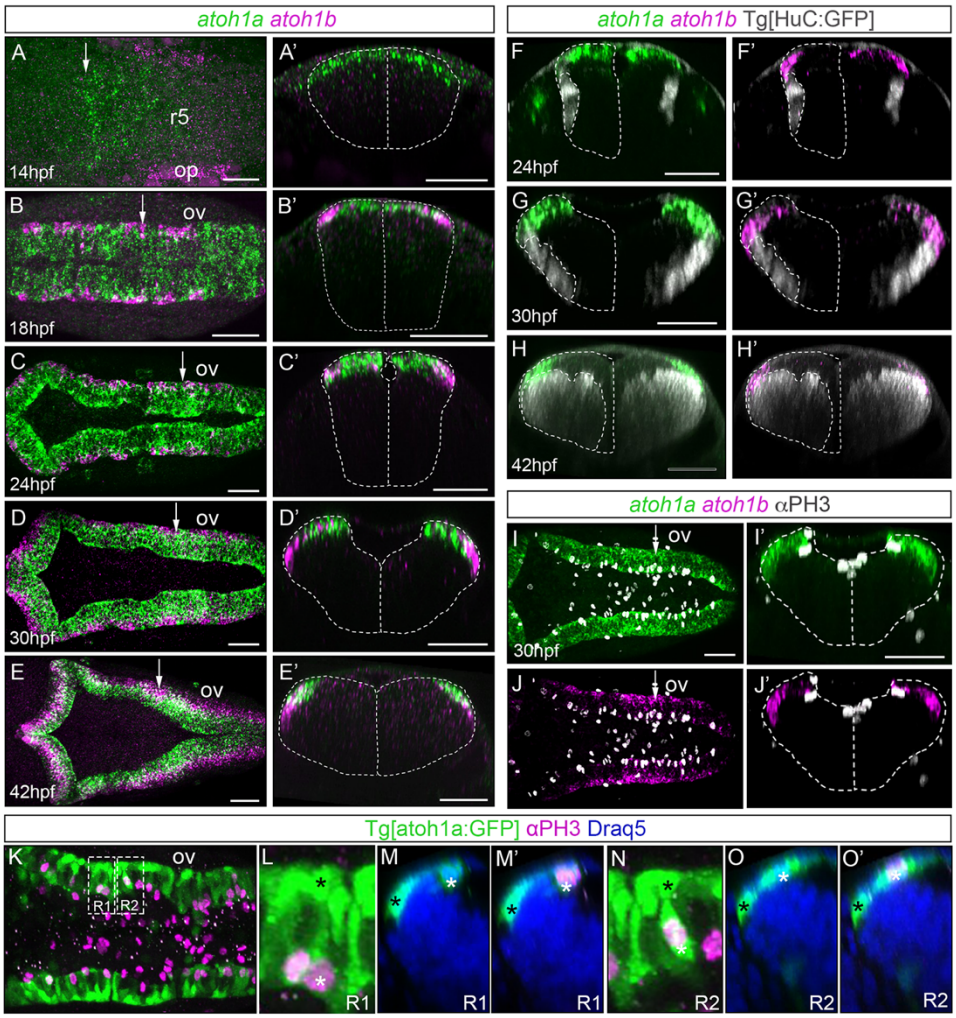
atoh1a atoh1b
A
r5
op
14hpf
A'
B
ov
18hpf
B'
C
ov
24hpf
C'
D
ov
30hpf
D'
E
ov
42hpf
E'
atoh1a atoh1b Tg[HuC:GFP]
F
24hpf
F'
G
30hpf
G'
H
42hpf
H'
atoh1a atoh1b αPH3
I
ov
30hpf
I'
J
ov
J'
Tg[atoh1a:GFP] αPH3 Draq5
K
ov
R1
R2
L
R1
M
R1
M'
R1
N
R2
O
R2
O'
R2

FIGURE 2

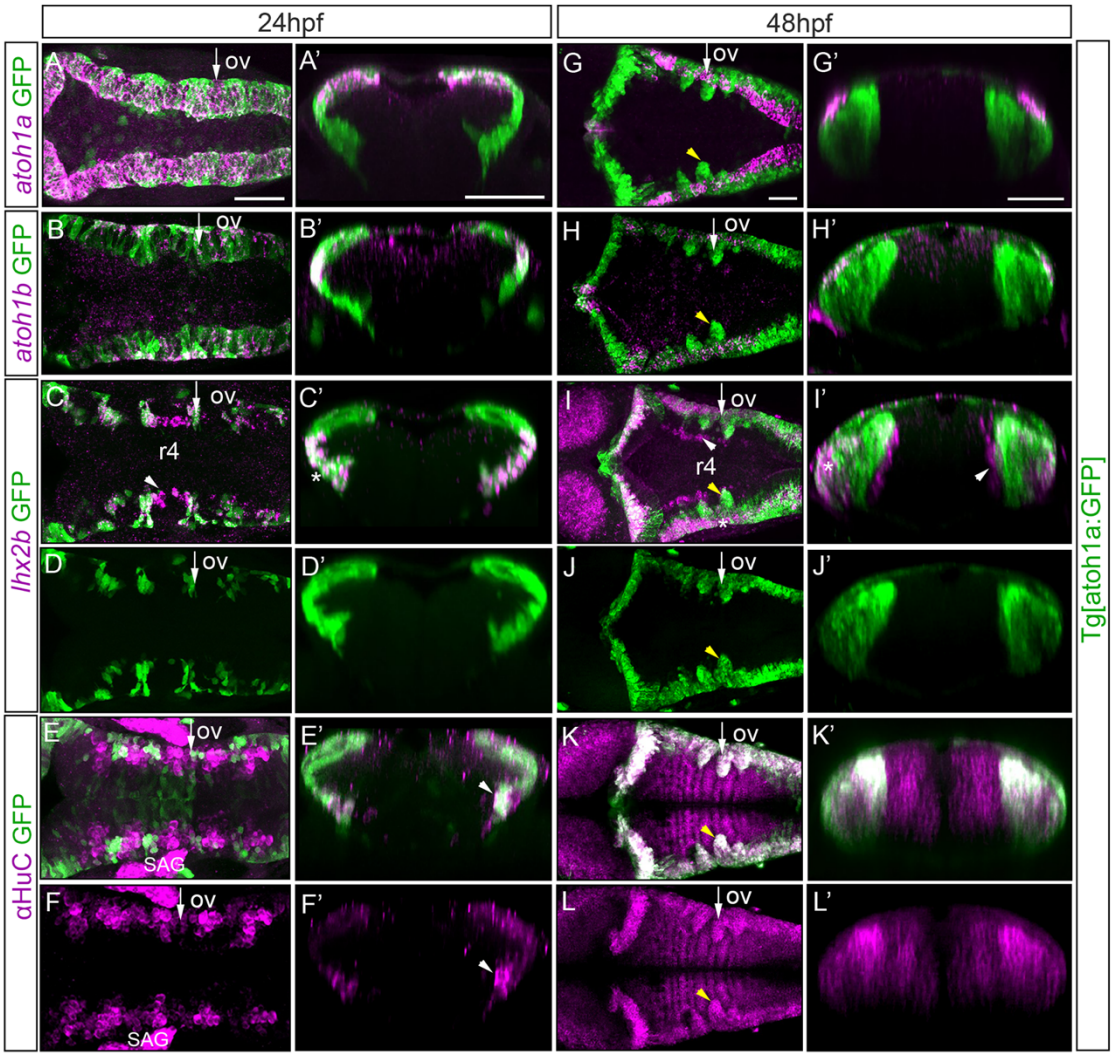
24hpf
48hpf
atoh1a GFP
atoh1b GFP
lhx2b GFP
αHuC GFP
Tg[atoh1a:GFP]
A
A'
G
G'
B
B'
H
H'
C
C'
I
I'
D
D'
J
J'
E
E'
K
K'
F
F'
L
L'
ov
r4
SAG

FIGURE 3

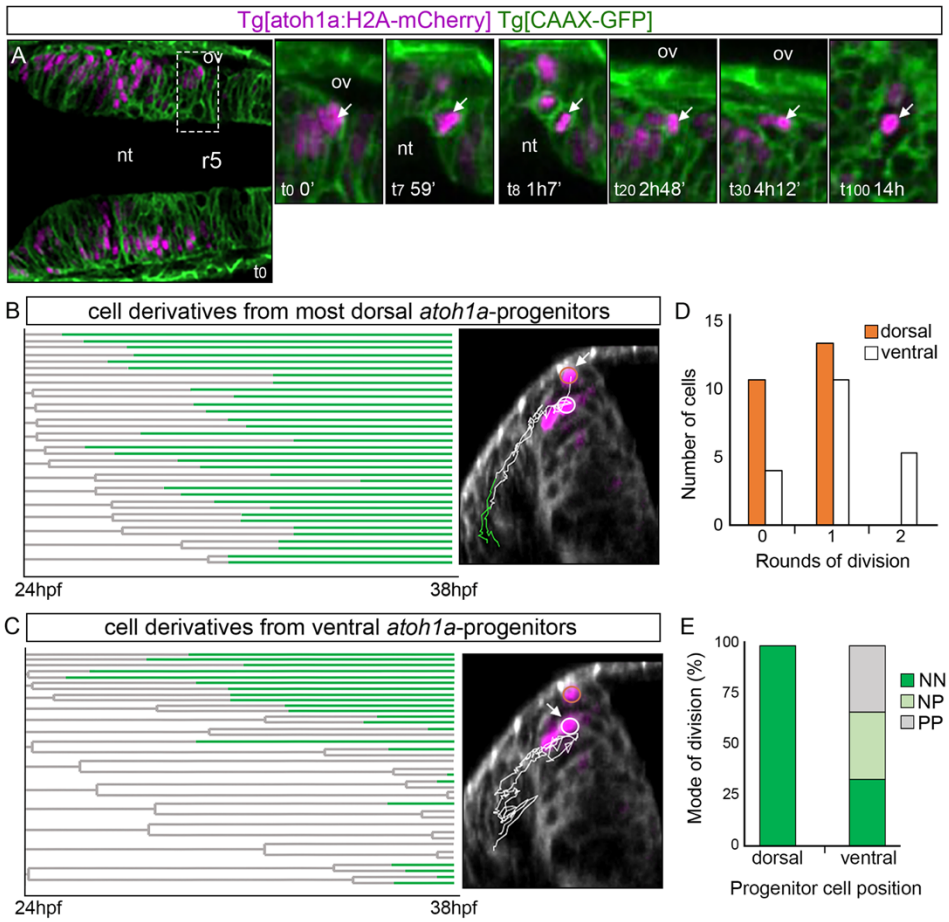
Tg[atoh1a:H2A-mCherry] Tg[CAAX-GFP]
A
ov
nt
r5
t0
t0 0'
t7 59'
t8 1h7'
t20 2h48'
t30 4h12'
t100 14h
B
cell derivatives from most dorsal atoh1a-progenitors
24hpf
38hpf
C
cell derivatives from ventral atoh1a-progenitors
24hpf
38hpf
D
Number of cells
Rounds of division
dorsal
ventral
E
Mode of division (%)
Progenitor cell position
dorsal
ventral
NN
NP
PP

FIGURE 4

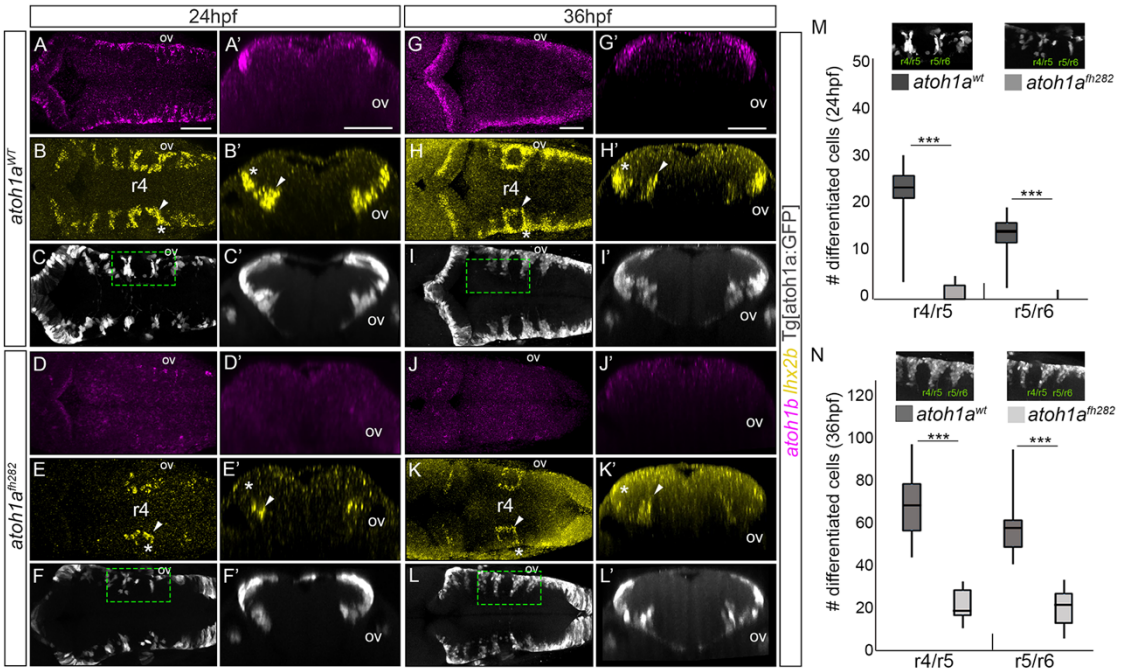
24hpf
36hpf
atoh1a^WT
atoh1a^fh282
atoh1b lhx2b Tg[atoh1a:GFP]
ov
r4
M
N
differentiated cells (24hpf)
differentiated cells (36hpf)
atoh1a^wt
atoh1a^fh282
r4/r5
r5/r6
***

FIGURE 5

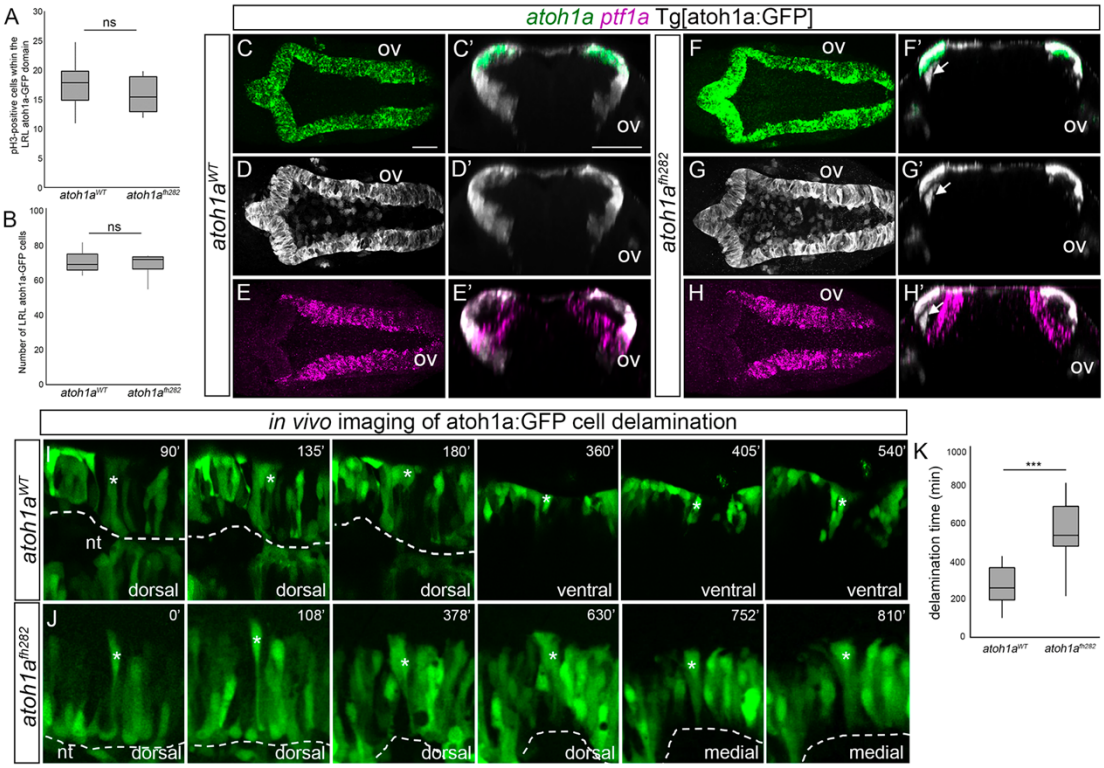
A
ns
pH3-positive cells within the LRL atoh1a-GFP domain
atoh1a^WT
atoh1a^fh282
B
ns
Number of LRL atoh1a-GFP cells
atoh1a^WT
atoh1a^fh282
atoh1a ptf1a Tg[atoh1a:GFP]
atoh1a^WT
atoh1a^fh282
C
C'
D
D'
E
E'
F
F'
G
G'
H
H'
ov
in vivo imaging of atoh1a:GFP cell delamination
atoh1a^WT
atoh1a^fh282
I
J
90'
135'
180'
360'
405'
540'
0'
108'
378'
630'
752'
810'
nt
dorsal
ventral
medial
K
***
delamination time (min)
atoh1a^WT
atoh1a^fh282

FIGURE 6

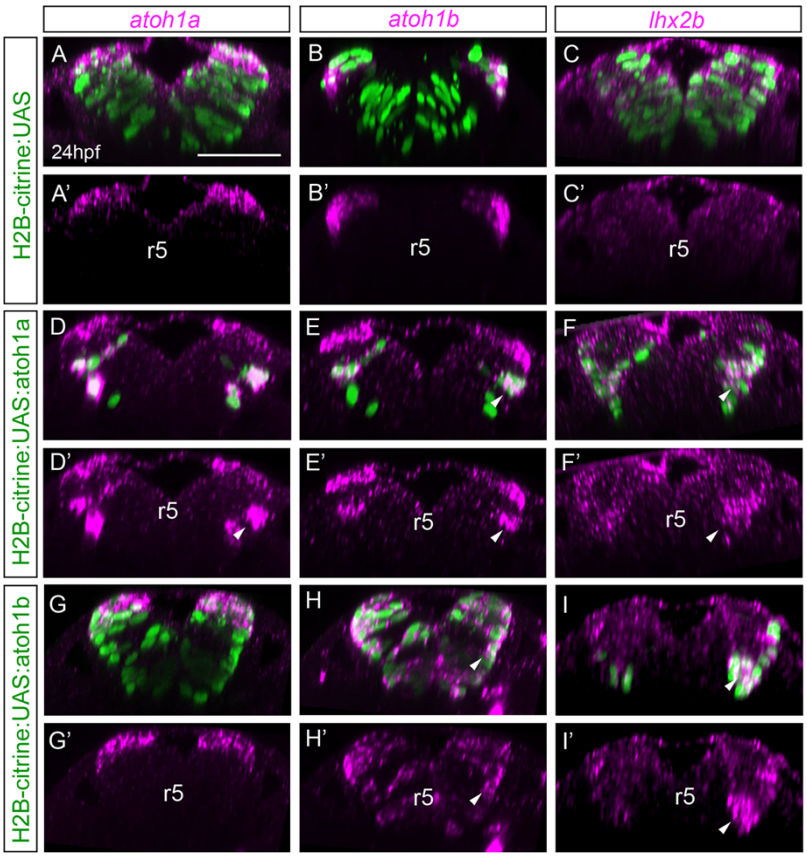
atoh1a
atoh1b
lhx2b
H2B-citrine:UAS
H2B-citrine:UAS:atoh1a
H2B-citrine:UAS:atoh1b
A
B
C
24hpf
A'
B'
C'
r5
D
E
F
D'
E'
F'
G
H
I
G'
H'
I'

FIGURE 7

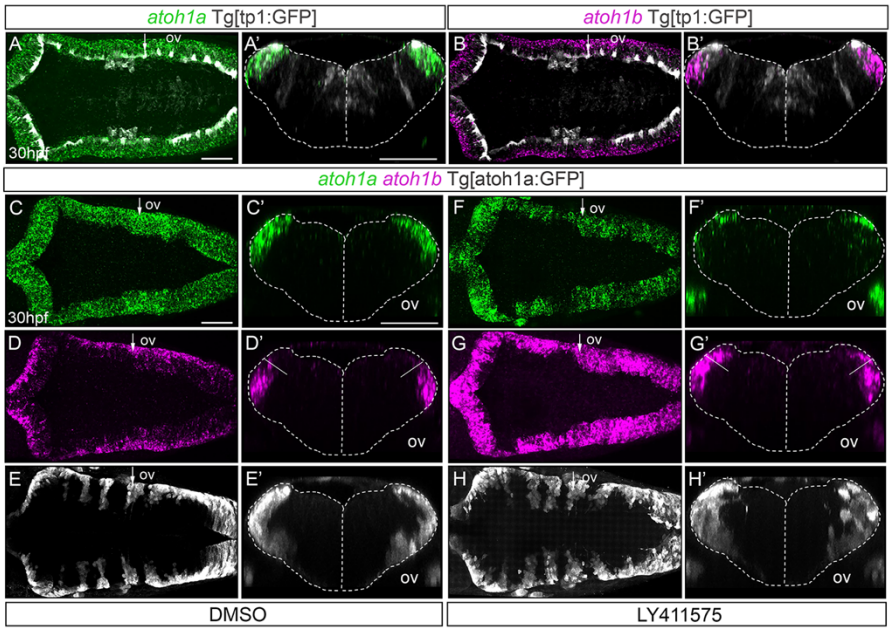
atoh1a Tg[tp1:GFP]
atoh1b Tg[tp1:GFP]
atoh1a atoh1b Tg[atoh1a:GFP]
A
A'
B
B'
C
C'
D
D'
E
E'
F
F'
G
G'
H
H'
ov
30hpf
DMSO
LY411575

FIGURE S1

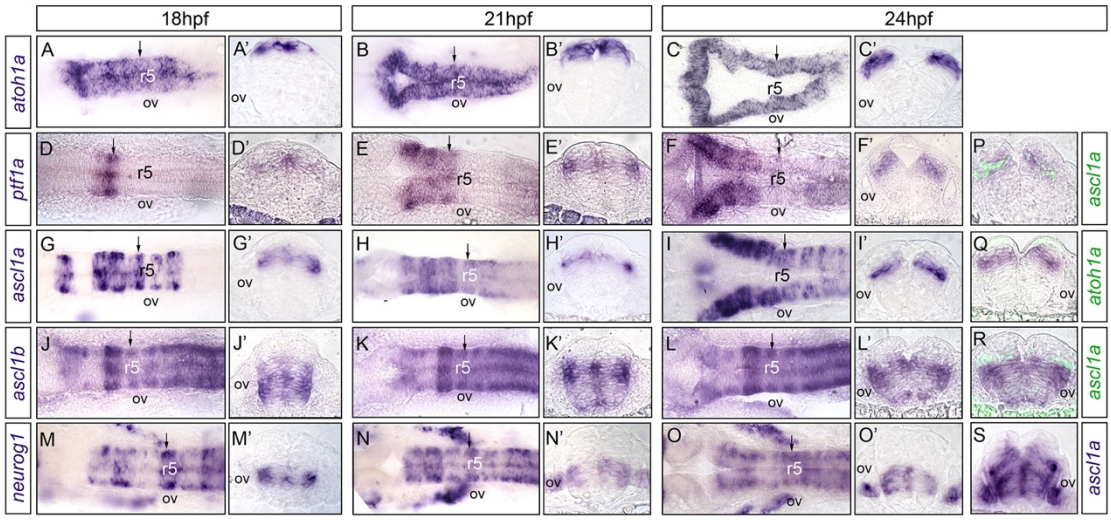
18hpf
21hpf
24hpf
atoh1a
ptf1a
ascl1a
ascl1b
neurog1
ascl1a
atoh1a
ascl1a
ascl1a
A
A'
B
B'
C
C'
D
D'
E
E'
F
F'
P
G
G'
H
H'
I
I'
Q
J
J'
K
K'
L
L'
R
M
M'
N
N'
O
O'
S
r5
ov

FIGURE S2

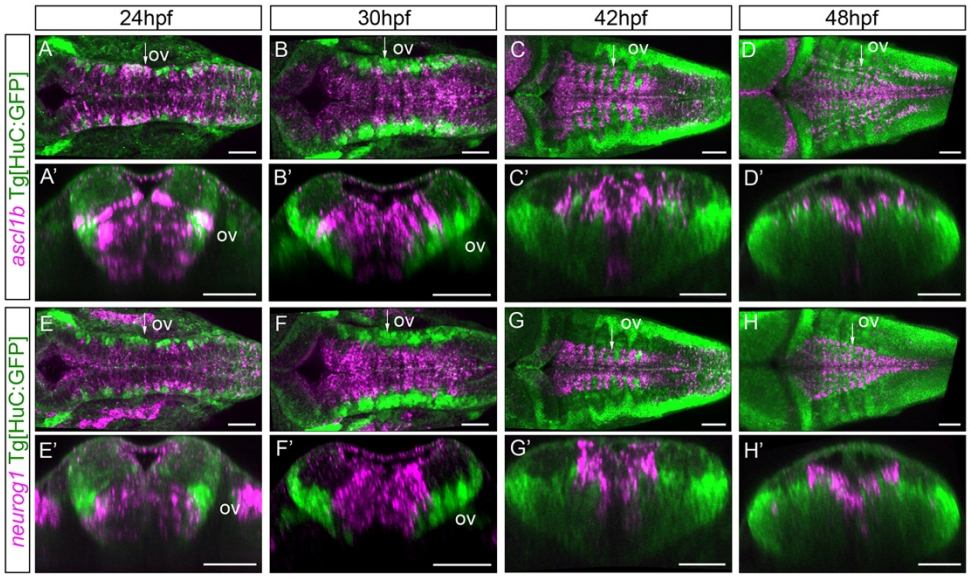
24hpf
30hpf
42hpf
48hpf
ascl1b Tg[HuC:GFP]
neurog1 Tg[HuC:GFP]
A
B
C
D
A'
B'
C'
D'
E
F
G
H
E'
F'
G'
H'
ov

FIGURE S3

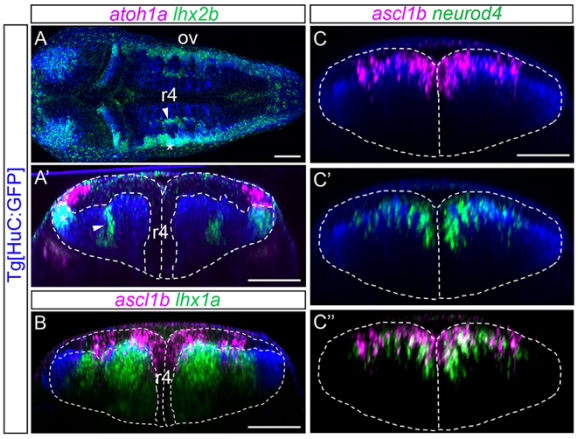
atoh1a lhx2b
ascl1b neurod4
ascl1b lhx1a
Tg[HuC:GFP]
A
ov
r4
A'
r4
B
r4
C
C'
C''

FIGURE S4

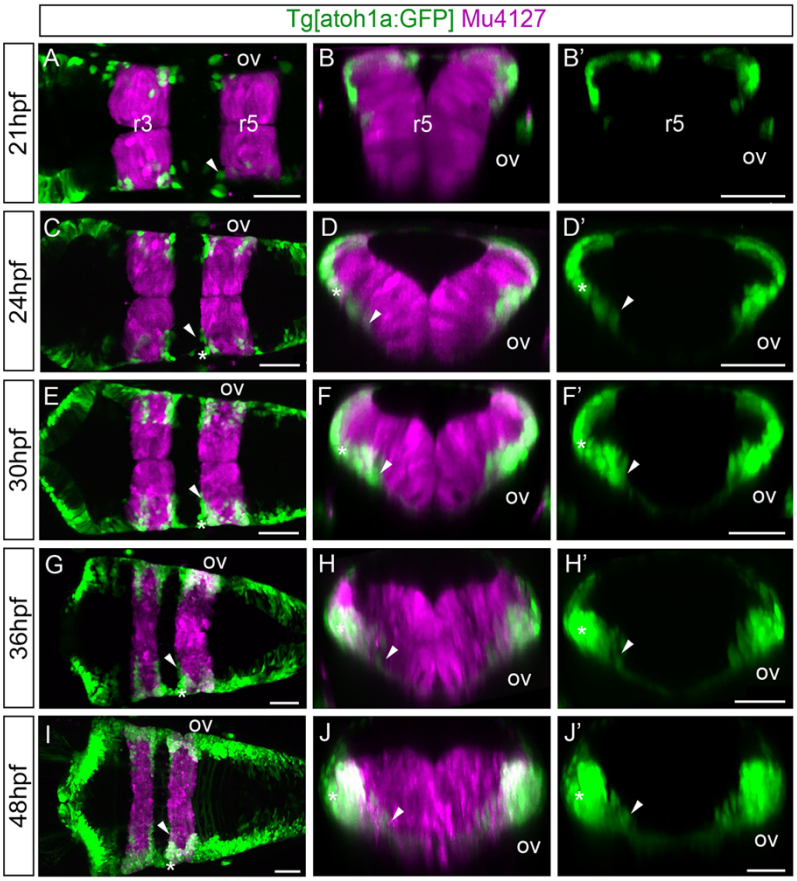
Tg[atoh1a:GFP] Mu4127
21hpf
24hpf
30hpf
36hpf
48hpf
A
B
B'
C
D
D'
E
F
F'
G
H
H'
I
J
J'
ov
r3
r5